Retention of function without normal disc morphogenesis occurs in cone but not rod photoreceptors

Rafal Farjo,[1] Jeff S. Skaggs,[1] Barbara A. Nagel,[2,3] Alexander B. Quiambao,[1] Zack A. Nash,[1] Steven J. Fliesler,[2,3] and Muna I. Naash[1]

[1]Department of Cell Biology, University of Oklahoma Health Sciences Center, Oklahoma City, OK 73104
[2]Department of Ophthalmology and [3]Department of Pharmacological and Physiological Science, Saint Louis University School of Medicine, St. Louis, MO 63104

It is commonly assumed that photoreceptor (PR) outer segment (OS) morphogenesis is reliant upon the presence of peripherin/rds, hereafter termed Rds. In this study, we demonstrate a differential requirement of Rds during rod and cone OS morphogenesis. In the absence of this PR-specific protein, rods do not form OSs and enter apoptosis, whereas cone PRs develop atypical OSs and are viable. Such OSs consist of dysmorphic membranous structures devoid of lamellae. These tubular OSs lack any stacked lamellae and have reduced phototransduction efficiency. The loss of Rds only appears to affect the shape of the OS, as the inner segment and connecting cilium remain intact. Furthermore, these structures fail to associate with the specialized extracellular matrix that surrounds cones, suggesting that Rds itself or normal OS formation is required for this interaction. This study provides novel insight into the distinct role of Rds in the OS development of rods and cones.

Introduction

The mammalian retina is comprised of both rod and cone photoreceptors (PRs), which initiate the phototransduction cascade upon excitation of their visual pigment by a photon of light. In both PR types, the outer segment (OS) is comprised of stacks of membranous discs in rods and lamellae in cones, which house and compartmentalize the proteins used in the phototransduction cascade. It is commonly thought that the proper development of these organelles is directly linked to normal PR cell function and viability; indeed, mutations in proteins specific to the OS (e.g., the rod visual pigment, rhodopsin) cause a multitude of blinding diseases (Molday, 1998). In both PRs, the plasma membrane undergoes further ultrastructural reorganization to form the discs of rod OSs and lamellae of cone OSs (Steinberg et al., 1980; Arikawa et al., 1992). In cones, the membrane lamellae are open and physically contiguous with the plasma membrane, whereas in rods, they become sealed, forming distinct membranous structures (discs) that are separated from the plasma membrane by cytosol. Rod and cone PRs also use redundant and analogous proteins for structural development and phototransduction, and many proteins have a conserved function in both PR cell types (Molday, 1998). The precise mechanism of OS morphogenesis is still a matter of active investigation even though the basic features of the process have been known for nearly 40 yr. However, a role for the PR-specific protein Rds (product of the retinal degeneration slow gene) in this process has been suggested based upon its localization to the disc rim, and in vitro data also suggest a fusogenic role for Rds in OS membrane assembly (Steinberg et al., 1980; Molday et al., 1987; Arikawa et al., 1992; Ritter et al., 2004; Damek-Poprawa et al., 2005).

Rds (also known as peripherin/rds or peripherin-2) is a tetraspanning transmembrane protein that is preferentially expressed in the OSs of rod and cone PRs (Molday et al., 1987; Connell and Molday, 1990; Wrigley et al., 2002). In the rod-dominated wild-type (WT) mouse retina, the loss of Rds causes a failure of OS generation, a greatly diminished response to light, and a slow degeneration of the PR cell layer (Sanyal et al., 1980; Sanyal and Jansen, 1981; Reuter and Sanyal, 1984; Jansen et al., 1987; Travis et al., 1989). However, these observations are limited by the fact that in the WT mouse retina, the PR population is comprised mostly of rods (>95%), making the study of cones difficult in this animal model. Although Rds is clearly requisite for normal rod OS morphogenesis and function, a similar requirement for Rds

Correspondence to Muna I. Naash: muna-naash@ouhsc.edu

Abbreviations used in this paper: CMS, cone matrix sheath; ERG, electroretinography; IS, inner segment; OS, outer segment; PNA, peanut agglutinin; PR, photoreceptor; qRT-PCR, quantitative RT-PCR; RPE, retinal pigment epithelium; WT, wild type.

The online version of this article contains supplemental material.

The Journal of Cell Biology, Vol. 173, No. 1, April 10, 2006 59–68
http://www.jcb.org/cgi/doi/10.1083/jcb.200509036

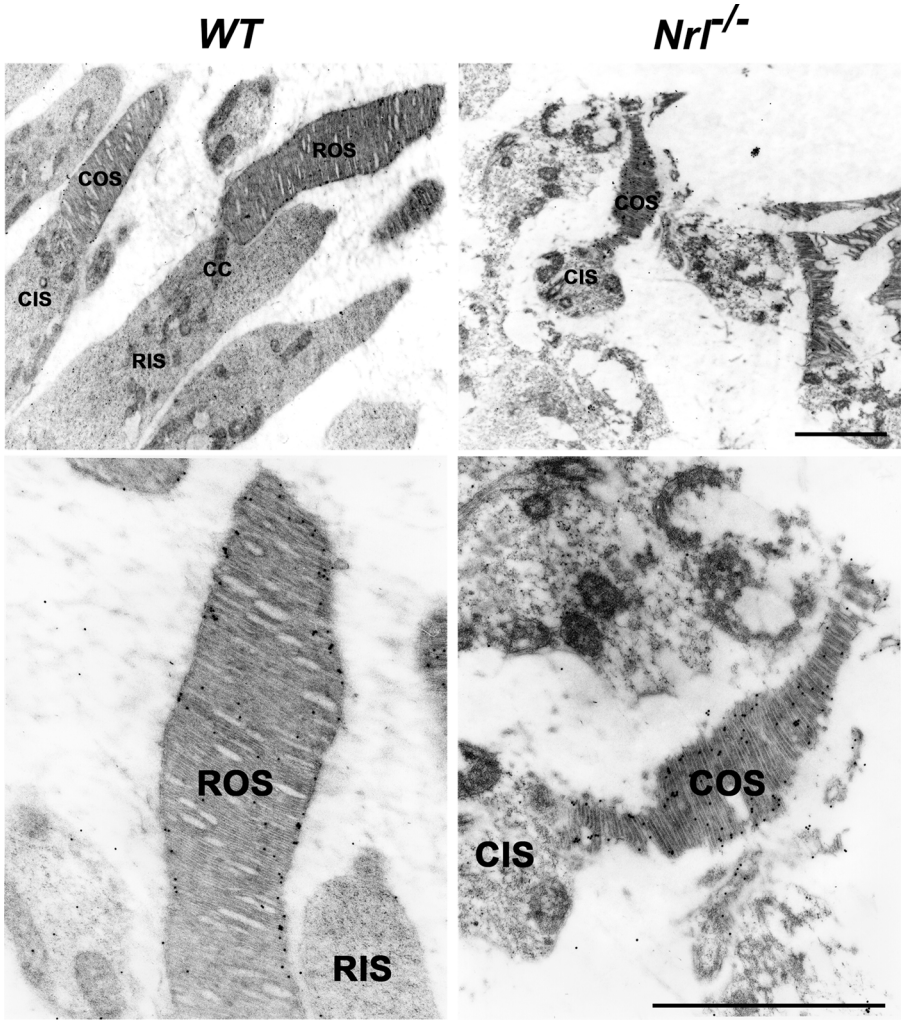

Figure 1. **Subcellular localization of Rds in WT and $Nrl^{-/-}$ retinas.** Immunogold labeling was performed to localize Rds immunoreactivity in WT and $Nrl^{-/-}$ retinas. Rds was present in the rim region of both rod and cone OSs in the WT retina and similarly observed in the cone OSs of the $Nrl^{-/-}$ retinas. CC, connecting cilium; CIS, cone inner segment; COS, cone outer segment; RIS, rod inner segment; ROS, rod outer segment. Bars, 2 μM.

in cone PRs has, as of yet, not been established. Furthermore, human mutations in Rds manifest as rod or cone dystrophies with varying severity (Kohl et al., 1998; van Soest et al., 1999; Musarella, 2001), suggesting this protein has distinct functions in rod and cone PRs.

Recently, a knockout of neural retina leucine zipper ($Nrl^{-/-}$) has been described in which rod PRs fail to develop and the retina consists entirely of cone PRs (Mears et al., 2001). Several studies have demonstrated the legitimacy and utility of the $Nrl^{-/-}$ mouse model as an excellent resource for studying cone PRs (Mears et al., 2001; Yoshida et al., 2004; Yu et al., 2004; Daniele et al., 2005; Nikonov et al., 2005). In this study, we took advantage of this model to assess the role of Rds in cone PRs, generating a double knockout mouse that lacked both Nrl and Rds ($Nrl^{-/-}/Rds^{-/-}$). We report that in the absence of Rds, cones form atypical OSs consisting of distended membranous structures that do not resemble morphologically normal lamellae. This is in striking contrast to rods, where no OSs form at all in the absence of Rds. Furthermore, these noncanonical cone OSs are capable of phototransduction with minimally reduced sensitivity, which is in marked contrast to the phenotype observed in the $Rds^{-/-}$ retina, where rod function is barely detectable. Finally, our results also suggest that Rds has a role in maintaining interactions between the OS and the specialized extracellular matrix that surrounds cone PRs (the so-called cone matrix sheath [CMS]; Hollyfield et al., 1989; Johnson et al., 1989; Hageman et al., 1995).

Results

Localization of Rds in $Nrl^{-/-}$ PRs

To examine the subcellular localization of Rds in cones, we used immunogold cytochemistry and ultrastructural analysis. The majority of Rds immunoreactivity was localized to the rim region of both rod and cone OSs in the WT retina, as previously observed (Fig. 1; Arikawa et al., 1992). A similar pattern of labeling was observed in the cone OSs of the $Nrl^{-/-}$ retina (Fig. 1), establishing the legitimacy of this model for studying Rds function in cones.

Differentiation status of $Nrl^{-/-}/Rds^{-/-}$ PRs

Successful crossbreeding of $Nrl^{-/-}$ and $Rds^{-/-}$ mice was verified with PCR genotyping (not depicted) and quantitative RT-PCR (qRT-PCR; Fig. 2 a). To determine the impact of the loss of Rds on PR differentiation, we used qRT-PCR to examine the mRNA levels of several genes involved in phototransduction and

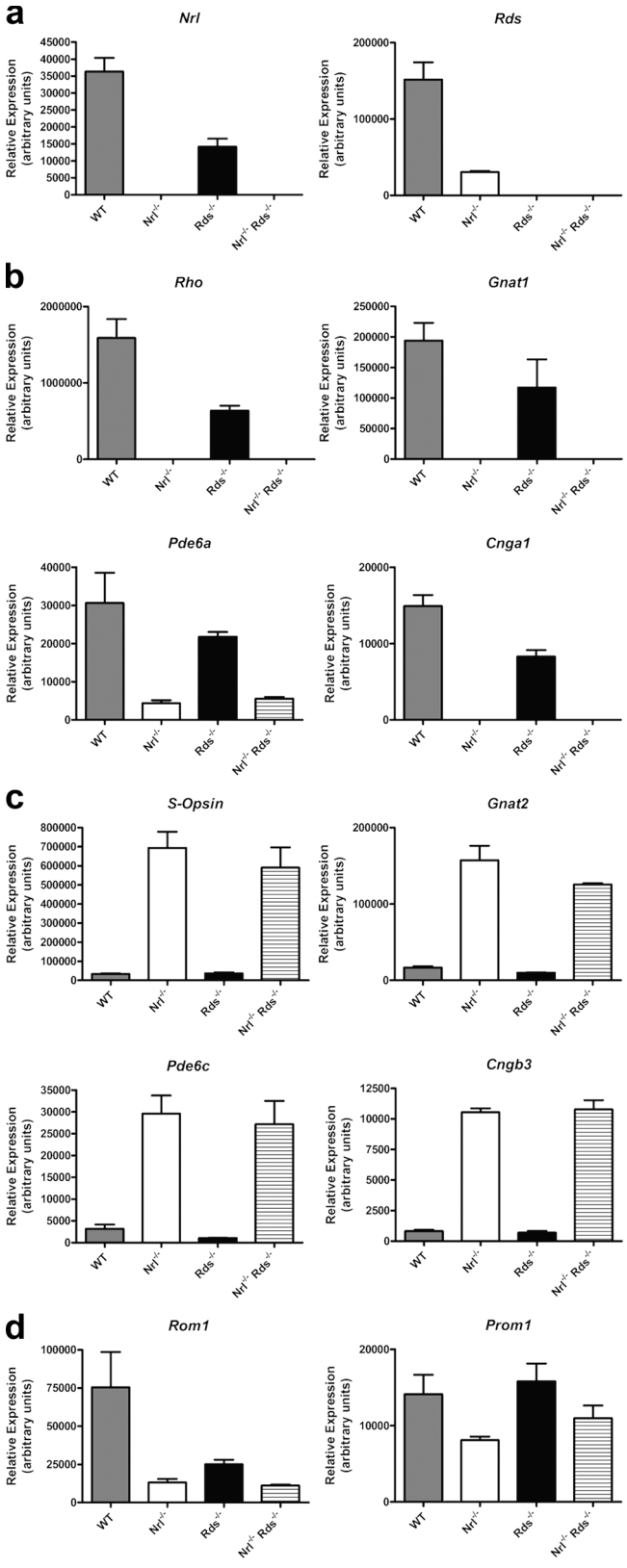

Figure 2. **Differentiation status of the *Nrl*$^{-/-}$/*Rds*$^{-/-}$ retina.** qRT-PCR was used to assess the expression levels of PR genes in P21 WT, *Nrl*$^{-/-}$, *Rds*$^{-/-}$, and *Nrl*$^{-/-}$/*Rds*$^{-/-}$ retinas. For all genes examined, comparable expression levels were observed in the *Nrl*$^{-/-}$ and *Nrl*$^{-/-}$/*Rds*$^{-/-}$ retinas. (a) Functional alleles of *Nrl* and *Rds* were absent in *Nrl*$^{-/-}$/*Rds*$^{-/-}$ as assayed with PCR primers flanking the site of genomic disruption in these two genes. (b) Rod-specific mRNAs were absent or significantly down-regulated in *Nrl*$^{-/-}$ and *Nrl*$^{-/-}$/*Rds*$^{-/-}$ retinas. Rhodopsin (*Rho*), rod-transducin (*Gnat1*), and rod cyclic nucleotide-gated channel α subunit (*Cnga1*) were highly expressed in the WT retina and to a lesser extent in the *Rds*$^{-/-}$ retina but were nearly undetectable in the retinas of *Nrl*$^{-/-}$ and *Nrl*$^{-/-}$/*Rds*$^{-/-}$ mice. Rod-specific phosphodiesterase (*Pde6a*) was also significantly down-regulated in the *Nrl*$^{-/-}$ and *Nrl*$^{-/-}$/*Rds*$^{-/-}$ retinas. (c) Cone-specific mRNAs were highly expressed in *Nrl*$^{-/-}$ and *Nrl*$^{-/-}$/*Rds*$^{-/-}$ retinas. The expression levels of S-opsin, cone transducin (*Gnat2*), cone phosphodiesterase (*Pde6c*), and cone cyclic nucleotide-gated channel β subunit (*Cngb3*) were significantly higher in the *Nrl*$^{-/-}$ and *Nrl*$^{-/-}$/*Rds*$^{-/-}$ retinas as compared with WT and *Rds*$^{-/-}$, demonstrating the overall enrichment of cone mRNAs in these models. (d) Genes involved in the maintenance of OS structure were not up-regulated to compensate for the loss of Rds. The expression levels of rod OS membrane protein 1 (*Rom1*) and prominin-1 (*Prom1*) were nearly equal in both the *Nrl*$^{-/-}$ and *Nrl*$^{-/-}$/*Rds*$^{-/-}$ retinas. Error bars represent SD.

maintenance of OS structure in the adult retina (Fig. 2, b–d). For all of the genes examined, similar expression levels were observed in the retinas of *Nrl*$^{-/-}$ and *Nrl*$^{-/-}$/*Rds*$^{-/-}$ mice. We detected no expression of rod opsin (*Rho*), rod transducin (*Gnat1*), or the rod cyclic nucleotide-gated channel (*Cnga1*) in either genetic background, and the level of rod phosphodiesterase (*Pde6a*) was substantially reduced as compared with WT and *Rds*$^{-/-}$ retinas (Fig. 2 b). In contrast, expression levels of cone phototransduction genes (*S-Opsin, Gnat2, Pde6c,* and *Cngb3*) were markedly increased in the *Nrl*$^{-/-}$/*Rds*$^{-/-}$ retinas relative to the WT retinas and were at comparable levels with those observed in the *Nrl*$^{-/-}$ retinas (Fig. 2 c; Mears et al., 2001; Yoshida et al., 2004; Yu et al., 2004). The expression levels of two retinal genes that produce proteins localized to the disc region of PR OSs were also examined. Rod OS membrane protein (*Rom-1*) and prominin-1 (*Prom-1*) were expressed at nearly identical levels in the *Nrl*$^{-/-}$ and *Nrl*$^{-/-}$/*Rds*$^{-/-}$ retinas (Fig. 2 d), indicating that these genes were not up-regulated to compensate for the loss of Rds.

Nrl$^{-/-}$/*Rds*$^{-/-}$ mice are capable of phototransduction

To evaluate retinal function in vivo, we used electroretinography (ERG) to examine the electrical response of the retina to light stimulation, distinguishing between rod and cone responses by varying the illuminance conditions before delivering a test flash. Multiple light intensities were used to stimulate light-adapted (photopic) WT, *Nrl*$^{-/-}$, *Rds*$^{-/-}$, and *Nrl*$^{-/-}$/*Rds*$^{-/-}$ mice at postnatal day 30 (P30; Fig. 3 a). Serial photopic ERGs demonstrated a complete absence of any electrical signal from the *Rds*$^{-/-}$ retina regardless of the light intensity. In the WT and *Nrl*$^{-/-}$ retinas, a b-wave signal was observed at −0.04 log cd sm^{-2} and enlarged with increasing flash intensities. A similar pattern of waveforms was detected in the *Nrl*$^{-/-}$/*Rds*$^{-/-}$ retina, starting at 0.37 log cd sm^{-2}, which is suggestive of reduced phototransduction sensitivity of nearly 1 log unit. Quantification at 1.89 log cd sm^{-2} revealed that photopic b-wave amplitudes were undetectable in *Rds*$^{-/-}$ mice but significantly higher in *Nrl*$^{-/-}$ and *Nrl*$^{-/-}$/*Rds*$^{-/-}$ mice as compared with the WT control (Fig. 3 b). It is likely that the lack of photopic ERG signal in *Rds*$^{-/-}$ mice results from either the toxic effect of the rapidly apoptosing rod PRs that is detrimental to the surviving cones or loss of the structural support of the rods. At this

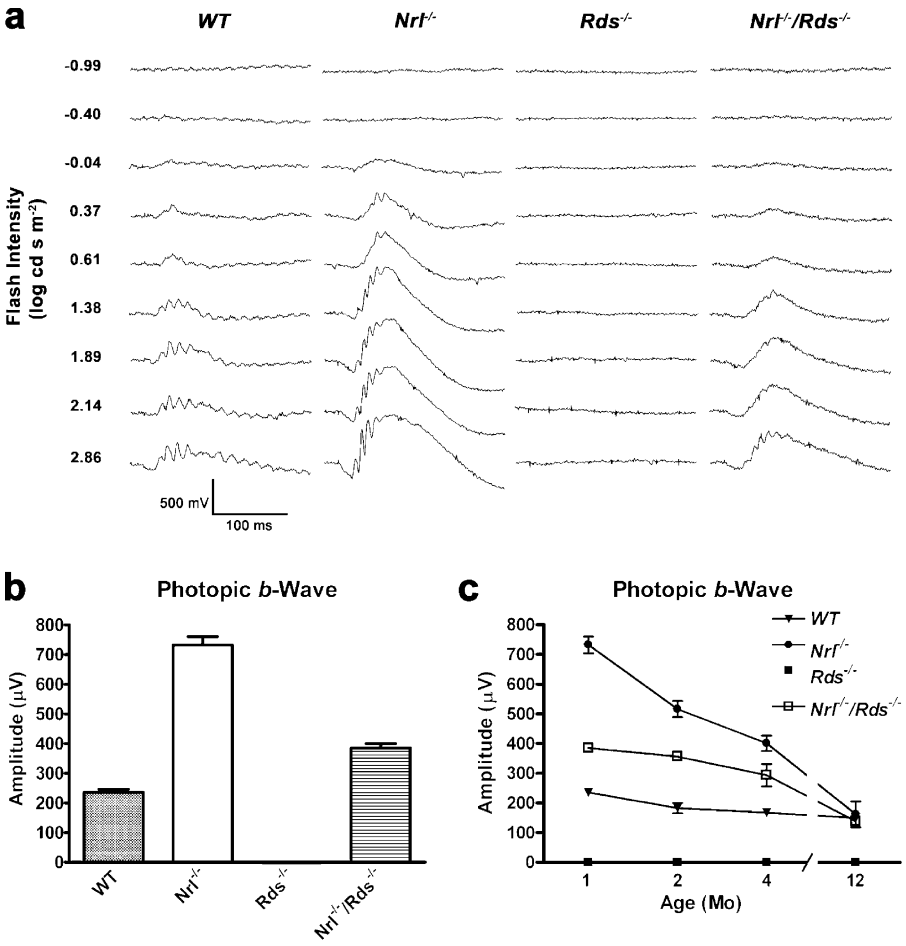

Figure 3. **Functional analysis of WT, $Nrl^{-/-}$, $Rds^{-/-}$, and $Nrl^{-/-}/Rds^{-/-}$ retinas.** Photopic ERGs were recorded after light adaptation to stimulate cone PR response. (a) Serial photopic ERG was performed with varying intensities of light stimuli on P30 mice, and the recorded waveforms are shown. At all light intensities, the $Rds^{-/-}$ waveforms were completely abolished; however, a-wave and b-wave amplitudes were observed in $Nrl^{-/-}/Rds^{-/-}$. ERG responses were detected and enlarged with increasing light stimuli starting at a flash intensity of −0.04 log cd s m^{-2} in the WT and $Nrl^{-/-}$ retinas and at 0.37 log cd s m^{-2} in the $Nrl^{-/-}/Rds^{-/-}$ retina. (b) Photopic ERGs were performed on P30 mice at a light intensity of 1.89 log cd s m^{-2}, and the b-wave was quantified. The b-wave amplitudes were significantly higher ($P < 0.001$) in $Nrl^{-/-}$ and $Nrl^{-/-}/Rds^{-/-}$ as compared with WT and $Rds^{-/-}$ mice. Specifically, mean b-wave values were as follows: WT = 235.6 (n = 12), $Nrl^{-/-}$ = 732.2 (n = 30), $Rds^{-/-}$ = 0 (n = 12), and $Nrl^{-/-}/Rds^{-/-}$ = 384.9 (n = 52). (c) Time course assessment of the photopic b-wave. A constant decline in the b-wave amplitude was observed in $Nrl^{-/-}$; however, no significant decrease was observed in $Nrl^{-/-}/Rds^{-/-}$ until P90. By 12 mo, the amplitudes were not significantly different from WT mice. Error bars represent SD.

intensity of light, $Nrl^{-/-}/Rds^{-/-}$ mice show nearly identical a- and b-waves regardless of whether scotopic (dark adapted) or photopic (light adapted) ERGs were recorded, signifying that the ERG responses of this mouse model originate in the cone PRs (Fig. S1, available at http://www.jcb.org/cgi/content/full/jcb.200509036/DC1). By 2 mo of age, the $Nrl^{-/-}$ photopic b-wave had decreased significantly, as previously reported (Daniele et al., 2005), and a declining trend in the photopic ERG amplitude of $Nrl^{-/-}/Rds^{-/-}$ was observed throughout the time course examined (Fig. 3 c). At 12 mo of age, the b-wave amplitudes of both strains were not significantly different from those recorded from age-matched WT mice. These data demonstrate that the retina of $Nrl^{-/-}/Rds^{-/-}$ is functionally cone dominated, similar to the $Nrl^{-/-}$ retina, and capable of significant levels of phototransduction, unlike the $Rds^{-/-}$ retina. We then hypothesized that the decreased photopic b-wave amplitude in $Nrl^{-/-}/Rds^{-/-}$ mice compared with that of $Nrl^{-/-}$ mice may represent altered phototransduction efficiency and sensitivity because of a structural abnormality resulting from the loss of Rds.

OS structure of cone PRs lacking Rds

To examine the localization of phototransduction and OS structural proteins, we used immunohistochemistry on retinal sections from P30 WT, $Nrl^{-/-}$, $Rds^{-/-}$, and $Nrl^{-/-}/Rds^{-/-}$ mice (Fig. 4 a). Rds immunoreactivity was abundant in the OS of both WT and $Nrl^{-/-}$ retinas but absent from $Rds^{-/-}$ and $Nrl^{-/-}/Rds^{-/-}$ retinas. The Rds-associated protein Rom-1 displayed an identical pattern of labeling as Rds, which is in support of previous observations that Rds is essential for Rom-1 targeting to the OS (Tam et al., 2004). Double labeling with monospecific primary antibodies revealed the presence of rod visual pigment (rhodopsin) and short wavelength cone visual pigment (S-opsin) in WT OSs and in the OS remnants of the $Rds^{-/-}$ retinas; however, retinas from $Nrl^{-/-}$ and $Nrl^{-/-}/Rds^{-/-}$ mice showed only S-opsin immunoreactivity localized in the subretinal space and rosettelike structures and retinal folds. To better define the morphology of the structures labeled by anti–S-opsin, thick sections (25 μM) were examined with confocal microscopy, and rotations of the image stacks were performed (Fig. 4 b). The OS of $Nrl^{-/-}$ retinas showed punctate labeling of tightly packed cone OS lamellae that were mostly aligned with the retinal pigment epithelium (RPE), which is typical of OS structure. However, in the $Nrl^{-/-}/Rds^{-/-}$ retina, a markedly different structure was observed. Instead of normal cone OSs, numerous tubular-shaped structures were located in the subretinal space, representing dysmorphic cone OSs. These structures were also longer than the punctate OS of $Nrl^{-/-}$ retinas and were not aligned with the RPE. Upon rotation of the image stack, a latticelike network of these structures was observed, possibly reflecting interactions between these OSs and the RPE microvilli.

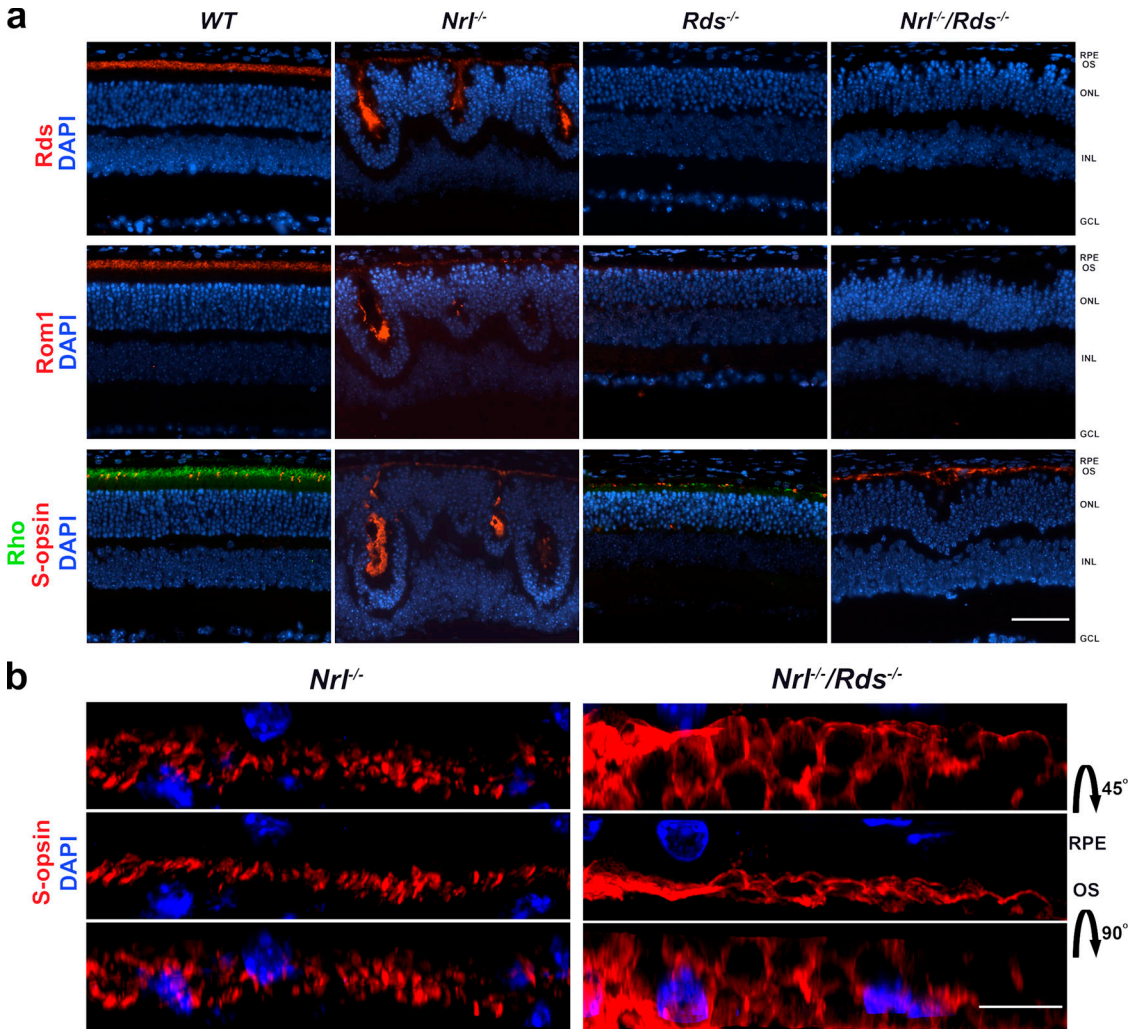

Figure 4. **Immunolocalization of OS proteins in the $Nrl^{-/-}/Rds^{-/-}$ retina.** Immunohistochemistry was performed on P30 WT, $Nrl^{-/-}$, $Rds^{-/-}$, and $Nrl^{-/-}/Rds^{-/-}$ retinas and imaged by indirect fluorescence microscopy. (a) Rds and Rom-1 were present in the OS layer of WT as well as in $Nrl^{-/-}$ rosettes but were undetectable in the $Rds^{-/-}$ and $Nrl^{-/-}/Rds^{-/-}$ sections. The WT retina was labeled by rhodopsin (green) and S-opsin (red), demonstrating the presence of both rods and cones, respectively. However, only S-opsin was observed in the $Nrl^{-/-}$ and $Nrl^{-/-}/Rds^{-/-}$ retinas, demonstrating that the retina of these models was dominated by cone PRs. Bar, 50 μM. (b) Immunohistochemistry to label cone S-opsin (red) was performed on P30 $Nrl^{-/-}$ and $Nrl^{-/-}/Rds^{-/-}$ retinas and imaged with laser scanning confocal microscopy. Images were shown after rotation of the image stack as depicted. Punctate labeling of the cone OS and lamellae structures was seen in the $Nrl^{-/-}$ retina, but a significantly different structure was observed in the $Nrl^{-/-}/Rds^{-/-}$ OS layer. These dysmorphic OSs appeared to have a tubular structure and form a latticelike network throughout the subretinal space. GCL, ganglion cell layer; INL, inner nuclear layer; ONL, outer nuclear layer; OS, outer segment; RPE, retinal pigment epithelium. Bar, 10 μM.

Rds is required for lamellae formation in cone OSs

Retinal histology and ultrastructure were evaluated by light and electron microscopy, respectively, using plastic-embedded tissue sections from P30 WT, $Nrl^{-/-}$, $Rds^{-/-}$, and $Nrl^{-/-}/Rds^{-/-}$ mice (Fig. 5). The characteristic heterochromatin clumps distinct to cone PR nuclei was noticeable in both $Nrl^{-/-}$ and $Nrl^{-/-}/Rds^{-/-}$ retinas (Fig. 5). The outer nuclear layer was well organized in the WT and $Rds^{-/-}$ retinas but was disrupted by whorls and rosette-like structures in the $Nrl^{-/-}$ retina and, to a lesser extent, in the $Nrl^{-/-}/Rds^{-/-}$ retina. $Nrl^{-/-}/Rds^{-/-}$ retinas exhibited an undulating morphology, with numerous retinal folds from the outer nuclear layer toward the inner nuclear layer, which failed to form complete rosettelike structures that were observed typically in retinas of $Nrl^{-/-}$ mice. Furthermore, retinas from $Nrl^{-/-}/Rds^{-/-}$ mice were prone to detachment from the RPE along many regions regardless of the fixation method used (not depicted). The lack of distinct rod OSs was apparent in all panels of Fig. 5 except those corresponding to retinas from WT eyes. Ultrastructural analysis demonstrated typical cone OS membrane structures in the $Nrl^{-/-}$ retina; however, dysmorphic membranous structures lacking the characteristic stacked cone OS lamellae were observed in $Nrl^{-/-}/Rds^{-/-}$ retinas. At a higher magnification, these lamellae-less OSs were distended and seemed to conform in shape to the space in which they were located (Fig. 5 b). Large balloon-shaped contiguous membrane structures also were observed, representing cone OSs that have failed to undergo normal morphogenesis. S-opsin immunoreactivity was detected solely in these membranous structures of the $Nrl^{-/-}/Rds^{-/-}$ retina (Fig. 5 c), further confirming their identity as cone OSs.

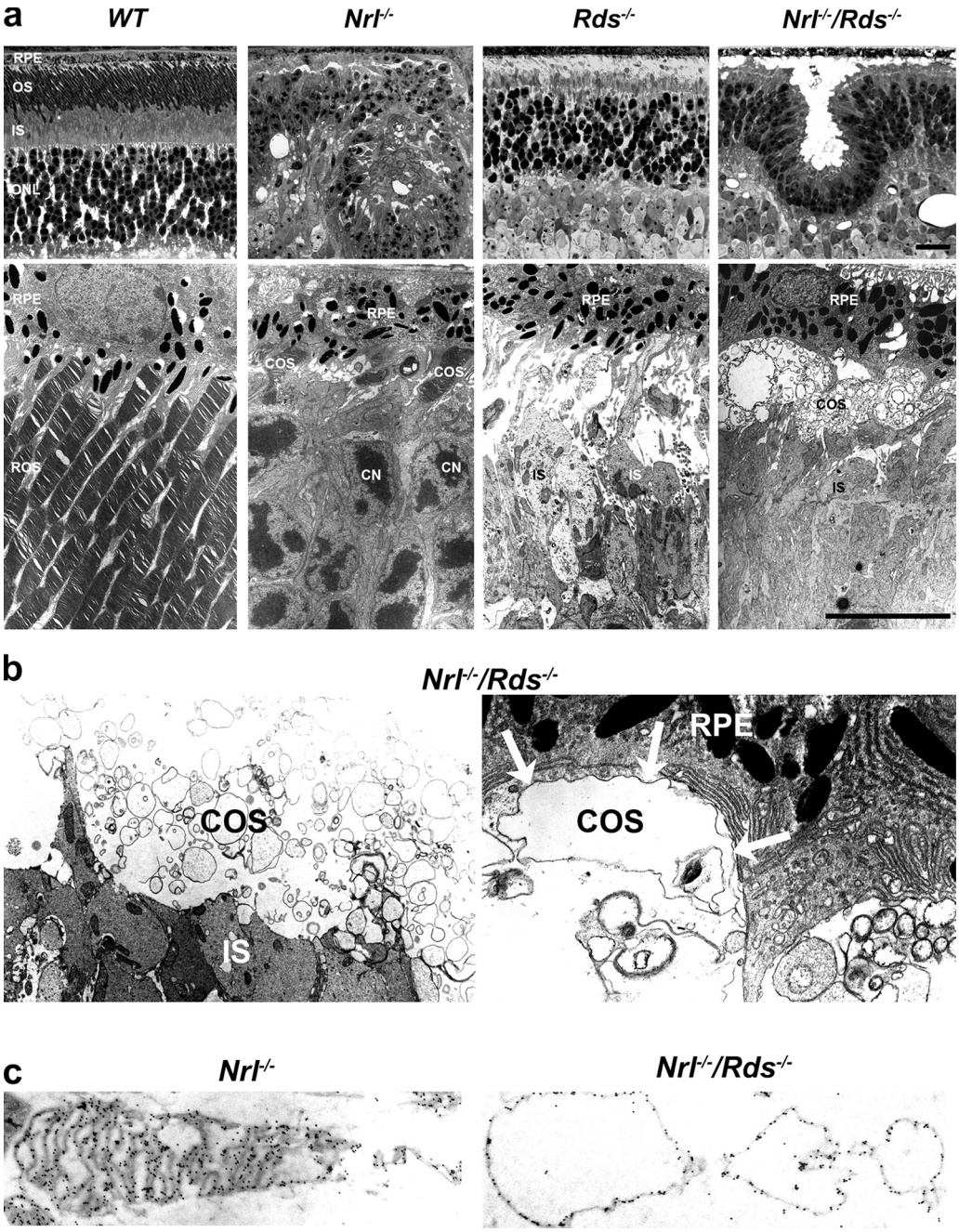

Figure 5. **Histological and ultrastructural analysis of OS morphology in *Nrl*$^{-/-}$*/Rds*$^{-/-}$.** (a) Representative light and electron microscopy images from P30 WT, *Nrl*$^{-/-}$, *Rds*$^{-/-}$, and *Nrl*$^{-/-}$*/Rds*$^{-/-}$ retinas. Characteristic OS structure was observed in WT panels and was completely absent from *Rds*$^{-/-}$ panels. Rosettelike structures and retinal folds were present in *Nrl*$^{-/-}$ and, to a lesser extent, in the *Nrl*$^{-/-}$*/Rds*$^{-/-}$ retinas. In contrast to the lamellae-containing OSs observed in *Nrl*$^{-/-}$, numerous wavy, membranous structures were observed in the OS layer of the *Nrl*$^{-/-}$*/Rds*$^{-/-}$ retina. Bars, 10 μM. (b) Ultrastructure images from the *Nrl*$^{-/-}$*/Rds*$^{-/-}$ retinas. The membranous OS structures appeared to lack the well-defined uniform organization of lamellae. At higher magnification, a single contiguous membrane appeared to be in contact with the RPE (arrows). (c) Immunogold detection of cone S-opsin in the *Nrl*$^{-/-}$ and *Nrl*$^{-/-}$*/Rds*$^{-/-}$ OS. S-opsin was present throughout the lamellae of the *Nrl*$^{-/-}$ retina, but only on the dysmorphic membrane structures of the *Nrl*$^{-/-}$*/Rds*$^{-/-}$ retina. CN, cone nucleus; COS, cone outer segment; IS, inner segment; ONL, outer nuclear layer; OS, outer segment; ROS, rod outer segment; RPE, retinal pigment epithelium.

Rds is required for interactions between the cone OS and the extracellular matrix

To further elucidate the cause of the abnormal morphology observed in the *Nrl*$^{-/-}$*/Rds*$^{-/-}$ retina, immunohistochemistry was performed to visualize PR-connecting cilia and inner segments (ISs) in the retinas of P30 mice (Fig. 6 a). The connecting cilium/axoneme and IS appeared intact in both models, as observed by labeling with antibodies to acetylated α-tubulin and to Na/K-ATPase, respectively. Hence, the loss of Rds resulted in gross structural changes in the OS but appeared to have no morphological effect on other PR structures or cellular compartments. We also examined localization of the CMS in relation to cone OSs (Fig. 6 b). This sheath surrounds the IS and OS of cone PRs to mediate adhesive interactions between the retina and

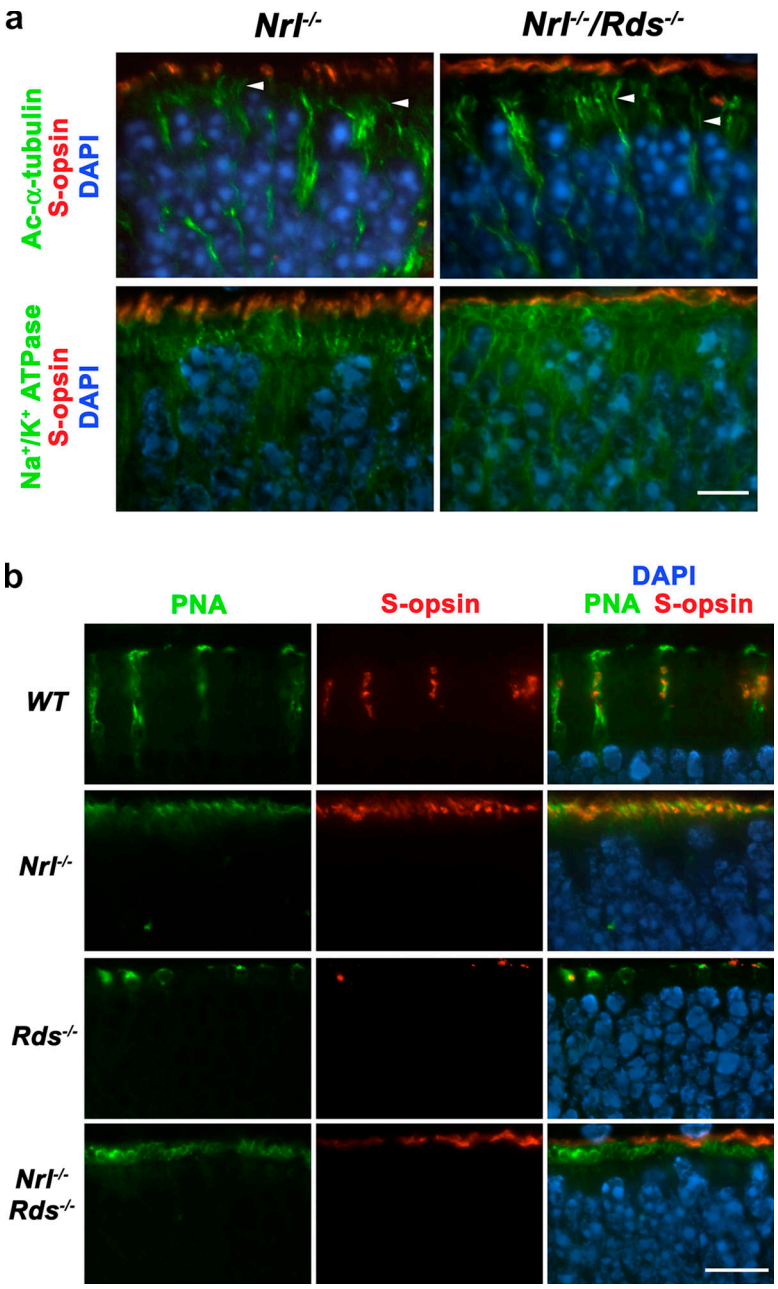

Figure 6. **Effect of Rds ablation on PR structure and extracellular matrix interactions.** Immunohistochemistry was performed on P30 retinas and imaged by indirect fluorescence microscopy. (a) The loss of Rds did not affect the morphology of the connecting cilium or IS in cone PRs. The PR-connecting cilium/axoneme and IS were visualized with antibodies against acetylated α-tubulin or Na/K-ATPase, respectively, and the OS was visualized with anti–s-opsin. The connecting cilium (arrowheads) and IS remained intact in $Nrl^{-/-}/Rds^{-/-}$, demonstrating that Rds ablation only affected the morphology of the OS. (b) Rds is necessary for proper interactions between the OS and the extracellular matrix. The cone extracellular matrix and OS were visualized by staining with PNA (AlexaFluor488 conjugated) and anti–S-opsin, respectively. In the WT and $Nrl^{-/-}$ panels, antibodies to S-opsin and fluorescently conjugated PNA label structures within the same layers of the retina and were found in the IS and OS. In $Nrl^{-/-}/Rds^{-/-}$, PNA staining was only present in the IS and does not overlap with S-opsin immunolabeling, demonstrating that OS interactions with the extracellular matrix are disturbed in this model. Bars, 10 μM.

RPE (Hollyfield et al., 1989; Johnson et al., 1989; Hageman et al., 1995). In retinal sections from WT and $Nrl^{-/-}$ mice, the CMS was labeled by fluorescently conjugated peanut agglutinin (PNA) and appeared within the IS and OS layers. Furthermore, S-opsin immunoreactivity was observed within the OS layer where PNA staining was detected. Interestingly, PNA labeling was not detected in the layer containing the dysmorphic cone-derived OS membranes of the $Nrl^{-/-}/Rds^{-/-}$ retina but was detected solely within the IS layer.

Discussion

In this study, we have demonstrated that the loss of Rds in cone PRs does not affect the differentiation of PRs but causes the formation of morphologically novel distended, membranous OS structures that, nonetheless, are capable of phototransduction. These structures contain S-opsin yet lack the compartmentalization of lamellae, directly implicating Rds in this process during cone OS morphogenesis. Rod PRs lacking Rds fail to form OS structures and possess rhodopsin solely in the tip of the cilium and IS membrane, causing minimal phototransduction activity and subsequent PR degeneration (Reuter and Sanyal, 1984; Nir and Papermaster, 1986). In contrast, cone PRs lacking Rds form altered OS structures lacking normal lamellar organization but, nonetheless, are capable of phototransduction, albeit with reduced sensitivity. Furthermore, the loss of Rds in cones with concomitant abortive lamellar formation prevents the extracellular matrix from forming around the cone OS, further reinforcing the notion that the OS lamellae are required for proper interactions between cone PRs and their extracellular environment.

In these studies, we have used the naturally occurring *rds* mutant mouse on a C57BL/6 background, and no photopic ERG signal is detectable using our methods. Previous investigations using *rds* mutant mice on a 020/A genetic background revealed a nominal scotopic ERG that would also include the response of surviving rods (Reuter and Sanyal, 1984). In that study, the ERGs may have been more sensitive, as they were performed by placing a needle electrode into the anterior chamber, whereas our method utilizes a looped platinum electrode placed on the cornea. These differences in genetic background and ERG methodology could explain the variation in results obtained between previous work (Reuter and Sanyal, 1984) and this study.

The data presented here support a model of cone OS membrane morphogenesis that predicts OS lamellae rim formation to be a second stage of morphogenesis after evagination of the plasma membrane from the connecting cilium (Steinberg et al., 1980). A previous study demonstrated ultrastructural localization of Rds in the rim regions in cones opposite to the connecting cilium where the membrane invaginates; however, in the rod PR, the OS plasma membrane is separated from the discs, and Rds localizes to the rim on both sides of the disc (Arikawa et al., 1992). Several studies have also shown the fusogenic properties of Rds (Boesze-Battaglia and Goldberg, 2002; Ritter et al., 2004; Damek-Poprawa et al., 2005), which further implicate its role in disc membrane morphogenesis. Based upon these models, we propose that the loss of Rds in cone PRs causes a morphogenic event in which plasma membrane evagination occurs but invagination fails, resulting in the formation of a dysmorphic OS organelle devoid of lamellae. Interestingly, these tubular-like OS membrane structures observed in the $Nrl^{-/-}/Rds^{-/-}$ retina are consistent with a model of cone OS morphogenesis by which growth of the plasma membrane occurs bidirectionally from the connecting cilium (Eckmiller, 1987). Further studies to reveal the subcellular compartmentalization of phototransduction proteins in this novel structure may reveal the exact purpose for the utilization of the disc membrane shape in the normal (WT) OS. This phenotype also demonstrates an inherently different role for Rds in rod versus cone PRs. It appears that cones only require Rds for membrane pinching to form the OS lamellae; however, in rods, Rds may have an additional role in OS development because its absence results in a more severe morphogenic outcome whereby the OS does not form and the rod PRs undergo apoptosis.

The disruption of CMS interactions with the dysmorphic OS as observed in the $Nrl^{-/-}/Rds^{-/-}$ retina suggests either a direct involvement of Rds in tethering the CMS to the OS or a more generalized dependence on normal OS structure for PR–matrix adhesional competence. The CMS is required for a variety of cell–matrix and cell–cell interactions, including trophic and metabolic interactions with the adjacent RPE (Hollyfield et al., 1989; Johnson et al., 1989; Hageman et al., 1995). The failed establishment of the CMS around these OSs suggests that disc morphogenesis (or normal OS formation) is somehow integrally linked to CMS association. Future biochemical studies to determine the precise role of Rds in the development and maintenance of this association may provide further insights into the compositional and functional differences between rod- and cone-associated extracellular matrix.

These observations also have implications regarding therapeutic strategies for treating human diseases involving Rds mutations that cause diseases specific to cone PRs. It is possible that a complete absence of Rds may be more advantageous than having mutant isoforms of Rds in cone PRs because human mutations in Rds that initially display cone-specific dysfunction could be caused by detrimental protein associations (e.g., aggregation of mutant Rds protein). In this regard, the use of RNA interference methodologies to silence *Rds* specifically in cone PRs may be a beneficial approach.

Materials and methods

Transgenic mice

All mice were bred into and assessed on a C57BL/6 background. All experiments and animal maintenance were approved by the local Institutional Animal Care and Use Committee (Oklahoma City, OK) and conformed to the guidelines on the care and use of animals adopted by the Society for Neuroscience and the Association for Research in Vision and Ophthalmology (Rockville, MD). The $Nrl^{-/-}$ mice were provided by A. Swaroop (University of Michigan Kellogg Eye Center, Ann Arbor, MI).

qRT-PCR

Total RNA was extracted from the retinas of a single mouse using TRIzol reagent (Invitrogen) and DNase treated with RNase-free DNase I (Promega). Reverse transcription was performed using an oligo-dT primer and Superscript III reverse transcriptase (Invitrogen). Primers for all genes were designed to span introns as to avoid amplification from genomic DNA. Primers for *Rds* spanned exon 2, where a 9-kb genomic insertion of a viral element causes the loss of Rds in the *rds* mouse, so amplification only occurred in those samples harboring a WT allele. All primer sequences are available in Table S1 (available at http://www.jcb.org/cgi/content/full/jcb.200509036/DC1). qRT-PCR was performed in triplicate on each cDNA sample using a real-time PCR detection system (iCycler; Bio-Rad Laboratories), and ΔcT values were calculated against the neuronal housekeeping gene hypoxanthine phosphoribosyltransferase (*Hprt*). *Hprt* was assigned an arbitrary expression level of 10,000, and relative gene expression values were calculated by the following calculation: relative expression = $10{,}000/2^{\Delta cT}$, where ΔcT = (gene cT – *Hprt* cT). This was repeated with three independent samples for each genotype, and the mean expression value is presented with the SD. Agarose gel electrophoresis and disassociation curve analysis were performed on all PCR products to confirm proper amplification.

ERG recordings

ERG analyses were performed as previously described (Cheng et al., 1997). In brief, after a minimum of 4-h dark adaptation, animals were anesthetized by intramuscular injection of 85 mg/kg ketamine and 14 mg/kg xylazine. For the assessment of scotopic response, a stimulus intensity of 1.89 log cd s m^{-2} was presented to the dark-adapted dilated eyes in a Ganzfeld (GS-2000; Nicolet). The amplitude of the scotopic a-wave was measured from the prestimulus baseline to the a-wave trough. The amplitude of the b-wave was measured from the trough of the a-wave to the crest of the b-wave. To evaluate photopic response, animals were light adapted for 5 min under a light source of 1.46 log cd m^{-2} intensity. Afterward, a strobe flash was presented to the dilated eyes in the Ganzfeld with various intensities (−0.99–2.86 log cd s m^{-2}). The amplitude of the photopic b-wave was measured from the trough of the a-wave to the crest of the b-wave. Significance was determined using one-way analysis of variance and post-hoc tests using Bonferroni's pairwise comparisons (Prism, version 3.02; GraphPad).

Immunohistochemistry

Tissue fixation and sectioning were performed as previously described (Stricker et al., 2005). In brief, eyes from P30 mice were enucleated and fixed in 4% PFA/PBS for 16 h before paraffin embedding. Tissue sections (10-μm thickness) were obtained with a microtome, deparaffinized, rehydrated as described previously (Nour et al., 2004), and blocked in 5% BSA/PBS for 30 min at RT. Slides were briefly washed with PBS and incubated with the primary antibody in 1× BSA/PBS for 2 h at RT followed

by a brief wash in PBS and incubation with the secondary antibody in 1× BSA/PBS for 30 min at RT. After a brief washing in PBS, Vectashield with DAPI (Vector Laboratories) was applied, and the slide was coverslipped. Primary antibodies (with dilutions) and sources were as follows: anti–Rds-CT (1:200); anti-Rom1 (1:200); monoclonal anti-rod opsin (Rho 1D4; 1:1,000) provided by R. Molday (University of British Columbia, Vancouver, Canada; Hicks and Molday, 1986); rabbit anti–mouse S-opsin (1:500), a gift from C. Craft and X. Zhu (Doheny Eye Institute, University of Southern California, Los Angeles, CA); acetylated α-tubulin (1:200) from Sigma-Aldrich; and anti–Na^+/K^+-ATPase (1:100) from the Developmental Studies Hybridoma Bank (University of Iowa, Iowa City, IA; Lebovitz et al., 1989). All secondary antibodies (FITC or Cy3 conjugates; Jackson ImmunoResearch Laboratories) were applied at a dilution of 1:1,000 from the original stock. Before incubation with antibodies against acetylated α-tubulin and Na^+/K^+-ATPase, antigen retrieval was performed by incubating slides in 10 mM citrate buffer, pH 3.0, for 30 min at 37°C followed by a brief rinsing in PBS. For PNA staining, AlexaFluor488-conjugated PNA (Invitrogen) was applied at a 1:200 dilution during the incubation with secondary antibody. Sections were viewed at RT with a microscope (Axioskop 50; Carl Zeiss MicroImaging, Inc.) in the autoexpose mode using a 40, 63, or 100× objective. Images were captured with a digital camera (Axiocam HR; Carl Zeiss MicroImaging, Inc.) using Axiovision 3.1 software (Carl Zeiss MicroImaging, Inc.).

Transmission electron microscopy, light microscopy (histology), and plastic-embedment immunogold cytochemistry

Methods used for tissue collection and processing for plastic-embedment light and electron microscopy and immunohistochemistry were as previously described (Stricker et al., 2005). For conventional light and electron microscopy, mice were perfused with 0.1 M sodium phosphate buffer, pH 7.4, containing 2% (vol/vol) PFA and 2% (vol/vol) glutaraldehyde; for plastic-embedment immunohistochemistry, the buffered fixative contained 2% PFA and 0.1% glutaraldehyde. For light microscopy, tissue sections (0.75–1-μm thickness) were viewed and photographed with a photomicroscope (BH-2; Olympus) in the autoexpose mode using a 20 or 60× DplanApo objective, and images were collected with a digital camera system (DXM-1200; Nikon). For electron microscopy, Spur's resin-embedded or (for immunogold) LR White–embedded tissue sections (silver–gold) were viewed with an electron microscope (100EX; JEOL). For immunohistochemistry, primary antibodies (see previous section) were used at a 1:10 dilution; secondary antibodies (AuroProbe 10-nm gold-conjugated goat anti–rabbit IgG; GE Healthcare) were used at a 1:50 dilution.

Online supplemental material

Table S1 presents primers that were designed to generate amplicons of 180–300 bp using Primer3 software (http://frodo.wi.mit.edu/cgi-bin/primer3/primer3_www.cgi). Fig. S1 shows mice that were dark adapted for a minimum of 4 h or light adapted for at least 5 min, and scotopic ERG analyses were performed as described above. Online supplemental material is available at http://www.jcb.org/cgi/content/full/jcb.200509036/DC1.

We thank Drs. Muayyad Al-Ubaidi, Alan J. Mears, and Sepideh Zareparsi for critical evaluation of the manuscript and Dr. Anand Swaroop for providing us with breeding pairs of *Nrl*$^{-/-}$ mice used in this study. We also thank Drs. Robert S. Molday, Cheryl Craft, and Xuemei Zhu for supplying antibodies used in this study.

This study was supported by grants from the National Institutes of Health (EY10609 to M.I. Naash, EY07361 to S.J. Fliesler, and Core Grant for Vision Research EY12190 to M.I. Naash), the Foundation Fighting Blindness (to M.I. Naash), the Norman J. Stupp Foundation Charitable Trust (to S.J. Fliesler), and by an unrestricted departmental grant from Research to Prevent Blindness (to S.J. Fliesler). M.I. Naash is a recipient of the Research to Prevent Blindness James S. Adams Scholar Award.

Submitted: 6 September 2005
Accepted: 2 March 2006

References

Arikawa, K., L.L. Molday, R.S. Molday, and D.S. Williams. 1992. Localization of peripherin/rds in the disk membranes of cone and rod photoreceptors: relationship to disk membrane morphogenesis and retinal degeneration. *J. Cell Biol.* 116:659–667.

Boesze-Battaglia, K., and A.F. Goldberg. 2002. Photoreceptor renewal: a role for peripherin/rds. *Int. Rev. Cytol.* 217:183–225.

Cheng, T., N.S. Peachey, S. Li, Y. Goto, Y. Cao, and M.I. Naash. 1997. The effect of peripherin/rds haploinsufficiency on rod and cone photoreceptors. *J. Neurosci.* 17:8118–8128.

Connell, G.J., and R.S. Molday. 1990. Molecular cloning, primary structure, and orientation of the vertebrate photoreceptor cell protein peripherin in the rod outer segment disk membrane. *Biochemistry*. 29:4691–4698.

Damek-Poprawa, M., J. Krouse, C. Gretzula, and K. Boesze-Battaglia. 2005. A novel tetraspanin fusion protein, peripherin-2, requires a region upstream of the fusion domain for activity. *J. Biol. Chem.* 280:9217–9224.

Daniele, L.L., C. Lillo, A.L. Lyubarsky, S.S. Nikonov, N. Philp, A.J. Mears, A. Swaroop, D.S. Williams, and E.N. Pugh Jr. 2005. Cone-like morphological, molecular, and electrophysiological features of the photoreceptors of the Nrl knockout mouse. *Invest. Ophthalmol. Vis. Sci.* 46:2156–2167.

Eckmiller, M.S. 1987. Cone outer segment morphogenesis: taper change and distal invaginations. *J. Cell Biol.* 105:2267–2277.

Hageman, G.S., M.F. Marmor, X.Y. Yao, and L.V. Johnson. 1995. The interphotoreceptor matrix mediates primate retinal adhesion. *Arch. Ophthalmol.* 113:655–660.

Hicks, D., and R.S. Molday. 1986. Differential immunogold-dextran labeling of bovine and frog rod and cone cells using monoclonal antibodies against bovine rhodopsin. *Exp. Eye Res.* 42:55–71.

Hollyfield, J.G., H.H. Varner, M.E. Rayborn, and A.M. Osterfeld. 1989. Retinal attachment to the pigment epithelium. Linkage through an extracellular sheath surrounding cone photoreceptors. *Retina*. 9:59–68.

Jansen, H.G., S. Sanyal, W.J. De Grip, and J.J. Schalken. 1987. Development and degeneration of retina in rds mutant mice: ultraimmunohistochemical localization of opsin. *Exp. Eye Res.* 44:347–361.

Johnson, L.V., J.C. Blanks, and G.S. Hageman. 1989. Effects of retinal degenerations on the cone matrix sheath. *Prog. Clin. Biol. Res.* 314:217–232.

Kohl, S., I. Giddings, D. Besch, E. Apfelstedt-Sylla, E. Zrenner, and B. Wissinger. 1998. The role of the peripherin/RDS gene in retinal dystrophies. *Acta Anat. (Basel)*. 162:75–84.

Lebovitz, R.M., K. Takeyasu, and D.M. Fambrough. 1989. Molecular characterization and expression of the (Na+ + K+)-ATPase alpha-subunit in *Drosophila melanogaster*. *EMBO J.* 8:193–202.

Mears, A.J., M. Kondo, P.K. Swain, Y. Takada, R.A. Bush, T.L. Saunders, P.A. Sieving, and A. Swaroop. 2001. Nrl is required for rod photoreceptor development. *Nat. Genet.* 29:447–452.

Molday, R.S. 1998. Photoreceptor membrane proteins, phototransduction, and retinal degenerative diseases. The Friedenwald Lecture. *Invest. Ophthalmol. Vis. Sci.* 39:2491–2513.

Molday, R.S., D. Hicks, and L. Molday. 1987. Peripherin. A rim-specific membrane protein of rod outer segment discs. *Invest. Ophthalmol. Vis. Sci.* 28:50–61.

Musarella, M.A. 2001. Molecular genetics of macular degeneration. *Doc. Ophthalmol.* 102:165–177.

Nikonov, S.S., L.L. Daniele, X. Zhu, C.M. Craft, A. Swaroop, and E.N. Pugh Jr. 2005. Photoreceptors of Nrl −/− mice coexpress functional S- and M-cone opsins having distinct inactivation mechanisms. *J. Gen. Physiol.* 125:287–304.

Nir, I., and D.S. Papermaster. 1986. Immunocytochemical localization of opsin in the inner segment and ciliary plasma membrane of photoreceptors in retinas of rds mutant mice. *Invest. Ophthalmol. Vis. Sci.* 27:836–840.

Nour, M., X.Q. Ding, H. Stricker, S.J. Fliesler, and M.I. Naash. 2004. Modulating expression of peripherin/rds in transgenic mice: critical levels and the effect of overexpression. *Invest. Ophthalmol. Vis. Sci.* 45:2514–2521.

Reuter, J.H., and S. Sanyal. 1984. Development and degeneration of retina in rds mutant mice: the electroretinogram. *Neurosci. Lett.* 48:231–237.

Ritter, L.M., K. Boesze-Battaglia, B.M. Tam, O.L. Moritz, N. Khattree, S.C. Chen, and A.F. Goldberg. 2004. Uncoupling of photoreceptor peripherin/rds fusogenic activity from biosynthesis, subunit assembly, and targeting: a potential mechanism for pathogenic effects. *J. Biol. Chem.* 279:39958–39967.

Sanyal, S., and H.G. Jansen. 1981. Absence of receptor outer segments in the retina of rds mutant mice. *Neurosci. Lett.* 21:23–26.

Sanyal, S., A. De Ruiter, and R.K. Hawkins. 1980. Development and degeneration of retina in rds mutant mice: light microscopy. *J. Comp. Neurol.* 194:193–207.

Steinberg, R.H., S.K. Fisher, and D.H. Anderson. 1980. Disc morphogenesis in vertebrate photoreceptors. *J. Comp. Neurol.* 190:501–508.

Stricker, H.M., X.Q. Ding, A. Quiambao, S.J. Fliesler, and M.I. Naash. 2005. The Cys214→Ser mutation in peripherin/rds causes a loss-of-function phenotype in transgenic mice. *Biochem. J.* 388:605–613.

Tam, B.M., O.L. Moritz, and D.S. Papermaster. 2004. The C terminus of peripherin/rds participates in rod outer segment targeting and alignment of disk incisures. *Mol. Biol. Cell*. 15:2027–2037.

Toda, K., R.A. Bush, P. Humphries, and P.A. Sieving. 1999. The electroretinogram of the rhodopsin knockout mouse. *Vis. Neurosci.* 16:391–398.

Travis, G.H., M.B. Brennan, P.E. Danielson, C.A. Kozak, and J.G. Sutcliffe. 1989. Identification of a photoreceptor-specific mRNA encoded by the gene responsible for retinal degeneration slow (rds). *Nature*. 338:70–73.

van Soest, S., A. Westerveld, P.T. de Jong, E.M. Bleeker-Wagemakers, and A.A. Bergen. 1999. Retinitis pigmentosa: defined from a molecular point of view. *Surv. Ophthalmol.* 43:321–334.

Wrigley, J.D., C.L. Nevett, and J.B. Findlay. 2002. Topological analysis of peripherin/rds and abnormal glycosylation of the pathogenic Pro216→Leu mutation. *Biochem. J.* 368:649–655.

Yoshida, S., A.J. Mears, J.S. Friedman, T. Carter, S. He, E. Oh, Y. Jing, R. Farjo, G. Fleury, C. Barlow, et al. 2004. Expression profiling of the developing and mature Nrl−/− mouse retina: identification of retinal disease candidates and transcriptional regulatory targets of Nrl. *Hum. Mol. Genet.* 13:1487–1503.

Yu, J., S. He, J.S. Friedman, M. Akimoto, D. Ghosh, A.J. Mears, D. Hicks, and A. Swaroop. 2004. Altered expression of genes of the Bmp/Smad and Wnt/calcium signaling pathways in the cone-only Nrl−/− mouse retina, revealed by gene profiling using custom cDNA microarrays. *J. Biol. Chem.* 279:42211–42220.